УДК 538.945

EFFECTS OF YTTRIUM OXIDE INCLUSIONS ON THE ORIENTATION AND SUPERCONDUCTING PROPERTIES OF YBCO FILMS

© 2013 Mikhail E. Moyzykh[1,2], Olga V. Boytsova [3], Vadim A. Amelichev [2], Sergey V. Samoilenkov [2,4], Igor F. Voloshin [5], Andrey R. Kaul [1,2], Bertrand Lacroix [6], Fabien Paumier [6], Rolly J. Gaboriaud [6]

[1] *Department of Chemistry, Moscow State University, Vorobievy Gory, 1, str. 3, 119991 Moscow, Russia*

[2] *SuperOx Company*

[3] *Department of Materials Science, Moscow State University*

[4] *Institute of High Temperatures RAS*

[5] *All-Russian Electrical Engineering Institute*

[6] *Pôle Poitevin de Recherche pour l'Ingénieur en Mécanique, Matériaux et Énergétique (PPRIMME), Departement de Physique et Mécanique des matériaux*

Received 20.04.2013

Abstract. The formation of Y_2O_3 secondary phase in the films of $YBa_2Cu_3O_7$ (YBCO) high-temperature superconductor is of large interest because Y_2O_3 inclusions can increase the critical current density (J_c) in YBCO films. We studied Y-rich and Y-poor YBCO films prepared by the MOCVD method. Y_2O_3 phase appeared in the Y-rich films as small (20x10 nm) oriented particles distributed throughout the YBCO films. It was found that at the same growth conditions Y-rich YBCO films grew highly *c*-oriented, whereas in the Y-poor films both *a*- and *c*-oriented YBCO grains were present. The Y-rich films exhibited better superconducting properties (J_c) because of better YBCO texture and magnetic flux pinning on the Y_2O_3 inclusions.

Keywords: MOCVD, epitaxy, lattice mismatch, ordered nanostructure, HT-superconductor

INTRODUCTION

Since the discovery of high temperature superconductors (HTS) with critical temperatures above 77 K, to increase the critical current density, J_c (that is the maximum current which can be drawn through HTS without destructing superconductivity), has become one of the most important tasks in this field.

The so-called coated conductors or second generation (2G) HTS tapes contain $RBa_2Cu_3O_{7-\delta}$ (RBCO, R = yttrium or rare earth elements) films as superconducting layers. The thickness of a HTS layer in a coated conductor architecture is in the order of 1 μm, therefore to increase the J_c of RBCO films is important for practical application of 2G HTS tapes. The super-current in RBCO can flow only along the CuO_2 planes, which are perpendicular to the crystallographic *c*-axis. This results in strongly anisotropic superconducting properties of RBCO [1], [2]. High J_c's are observed when RBCO films grow with the RBCO *c*-axis perpendicular to the substrate surface (*c*-oriented RBCO). Growth of RBCO films with other axial orientations (usually with *a*-axis perpendicular to the substrate surface - *a*-oriented RBCO) reduces superconducting current along the substrate surface and results in the formation of grain boundaries that decrease superconducting properties even further [3]. Possible growth orientations in RBCO epitaxial films are shown in Fig. 1, using YBCO as an example. It has been recognized that non-superconducting nanosized R_2O_3 particles distributed within the matrix of RBCO film can increase J_c due to the formation of defects, which act like pinning centers [4—7] by stopping (pinning) magnetic flux creep in the superconductor. The orientation of Y_2O_3 particles in the YBCO matrix is also shown in Fig. 1.

In this work we aimed to clarify the relationship between the formation of *a*-oriented YBCO and the presence of Y_2O_3 particles in YBCO films, and to study the effect of Y_2O_3 particles on the J_c of YBCO films.

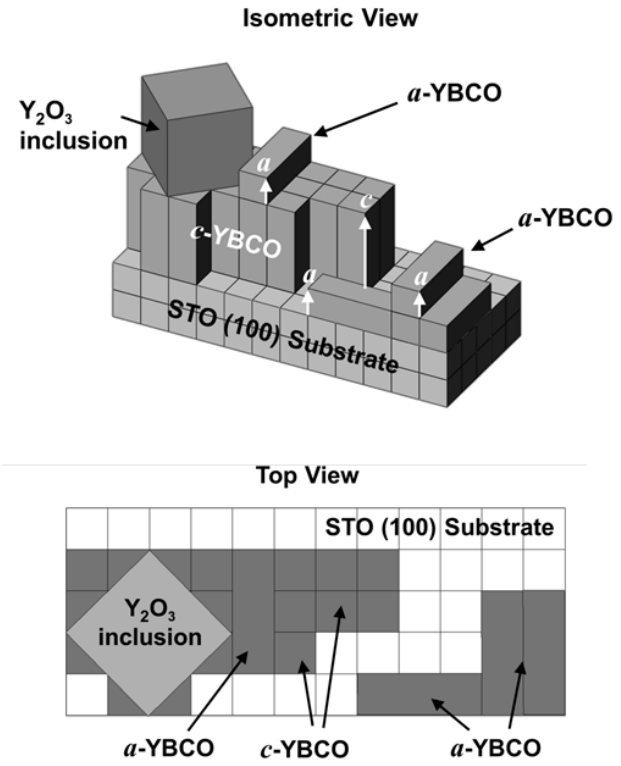

Fig. 1. Crystallographic orientation of YBCO and Y_2O_3 inclusions within the YBCO matrix in an yttrium-rich epitaxial YBCO film on $SrTiO_3$ substrate

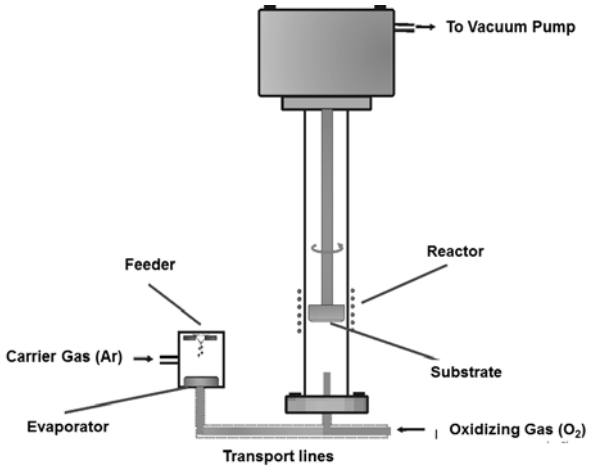

Fig. 2. Schematic drawing of the MOCVD system

EXPERIMENTAL SECTION

FILM DEPOSITION

Epitaxial YBCO films were grown via the MOCVD (Metal-Organic Chemical Vapor Deposition) technique on (100) $SrTiO_3$ (STO) single crystal substrates. The schematic drawing of the MOCVD system used for film deposition is shown in Fig. 2. The MOCVD precursor compounds used were $Y(thd)_3$, $Ba(thd)_2 \cdot 2Phen$, and $Cu(thd)_2$ (Hthd = 2,2,6,6-thetramethylheptanedion-3,5; Phen = *o*-Phenatroline). Microportions (~ 1 microgram) of a mixture of the three precursors were introduced into the pre-heated evaporator from the mechanical feeder unit. Precursor vapor was transported by Ar gas via heated lines to the vertical hot-wall quartz reactor, where the precursors mixed with oxygen and decomposed at the heated substrate forming a metal oxide film. Cation composition of the films was controlled by varying the amount of the yttrium precursor in the initial precursor mixture.

The substrate temperature T_s was controlled with the accuracy of ±2 °C in the 800—860 ºC range. Partial oxygen pressure, $p(O_2)$, was kept at 0.5 mbar, with total pressure of 2.5 mbar. After deposition the films were annealed at 450 ºC in 1 bar of oxygen, to increase the oxygen content of YBCO. The post-deposition oxygenation annealing resulted in films of orthorhombic $YBa_2Cu_3O_{7-\delta}$ with $\delta < 0.1$ (YBCO c-lattice parameter 11.680—11.700 Å).

Some films after oxygenation at 450 ºC in 1 bar of oxygen and characterization were reduced by annealing at 450 ºC in 1 bar of Ar for 60 minutes, and then re-oxygenated at 450 ºC in 1 bar of oxygen, to study stress and relaxation processes in the films.

Film thickness determined by RBS was in the 200—250 nm range.

FILM CHARACTERIZATION

Phase composition, lattice parameters and phase orientation were studied by X-ray diffraction (XRD) performed with Rigaku SmartLab diffractometer (CuK_α radiation, Ge monochromator) using the θ-2θ, φ- and 2θ-φ-χ-scanning techniques.

Film surface morphology was studied by scanning electron microscopy (SEM) using LEO Supra 50VP microscope (acceleration voltage – 20 kV, magnification 5000—100000).

Rutherford backscattering (RBS) measurements were used to estimate the film thickness, and they were performed using an EG-8 device with a semiconductor α-particle detector (2 mm ion beam diameter at the sample, 160º scattering angle, 2.0—2.5 keV per detector channel, 2000 sec spectrum collection time). We used SIMNRA 6.03 software for spectrum fit.

Phase composition and morphology across the film cross-section were studied with high resolution electron microscopy (HREM). HREM studies were performed with JEOL 3010 ARP microscope (300 kV operating voltage, up to $6 \cdot 10^5$ magnification) at Pôle Poitevin de Recherche pour l'Ingénieur en Mécanique,

Matériaux et Énergétique (PPRIMME), Departement de Physique et Mécanique des matériaux.

To characterize the superconducting properties of the thin film materials, AC magnetic susceptibility measurements were performed using APD-Cryogenics AC magnetometer. J_c values were calculated using the widths of the obtained magnetization loops and sample dimensions according to the Bean model of critical state.

RESULTS AND DISCUSSION

PHASE COMPOSITION OF THE FILMS

A typical XRD θ-2θ-scan of a near-stoichiometric YBCO film is shown in Fig. 3, revealing the following phases: YBCO (both *c*- and *a*-oriented), Y_2O_3, $YCuO_2$, $BaCuO_2$, and CuO. Although seemingly thermodynamically impossible, the situation with too many phases present simultaneously in near-stoichiometric YBCO films, especially in those grown by the incongruent MOCVD method, is quite common. Particles of various secondary phases, which often belong in different phase fields on the equilibrium phase diagram, form because of local and temporary compositional fluctuations during the growth and then get spatially separated from each other in the crystallized film.

We designated a phase ratio as the intensity of the strongest reflections of the respective phase: (200) for *a*-oriented YBCO (*a*-YBCO), (400) for Y_2O_3, (660) for $BaCuO_2$ and (005) for *c*-oriented YBCO (*c*-YBCO). For all samples, the intensities were normalized to the intensity of the *c*-oriented YBCO (005)-reflection, in order to compensate for the film thickness variation:

$$I_n(a\text{-YBCO}) = I[(200)\text{YBCO}]/I[(005)\text{YBCO}]\ (\%)$$

$$I_n(Y_2O_3) = I[(400)Y_2O_3]/I[(005)\text{YBCO}]\ (\%)$$

$$I_n(BaCuO_2) = I[(660)BaCuO_2]/I[(005)\text{YBCO}]\ (\%)$$

The YBCO films were preferentially *c*-oriented, growing epitaxially in the "cube-on-cube" mode (see φ-scans in Fig. 4), which is typical for YBCO growth on (100) STO. The (100) and (200) reflections of *a*-oriented YBCO were also observed in the θ-2θ-scans, in some films the intensity of the *a*-oriented YBCO XRD reflections reaching up to 50% of that of the *c*-oriented YBCO reflections.

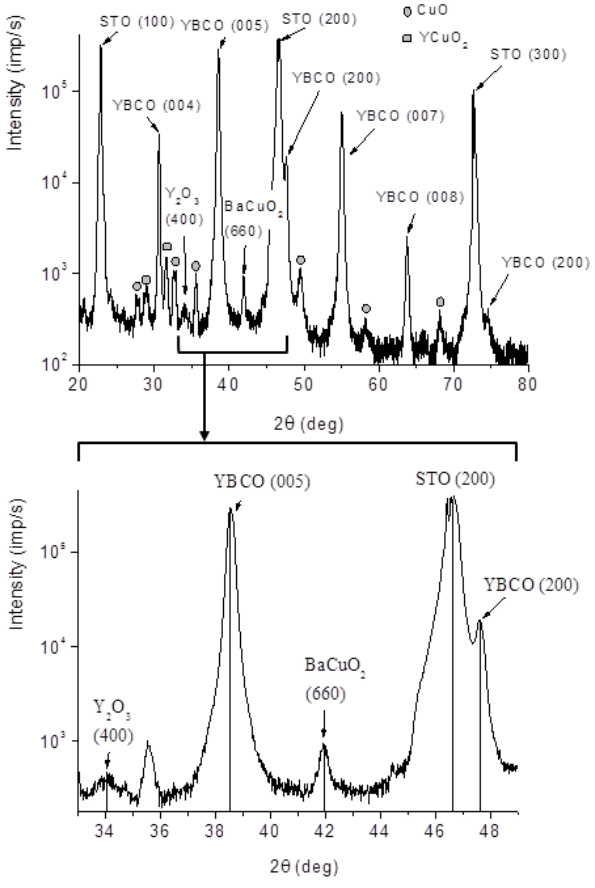

Fig. 3. Typical XRD pattern of a near-stoichiometric YBCO film

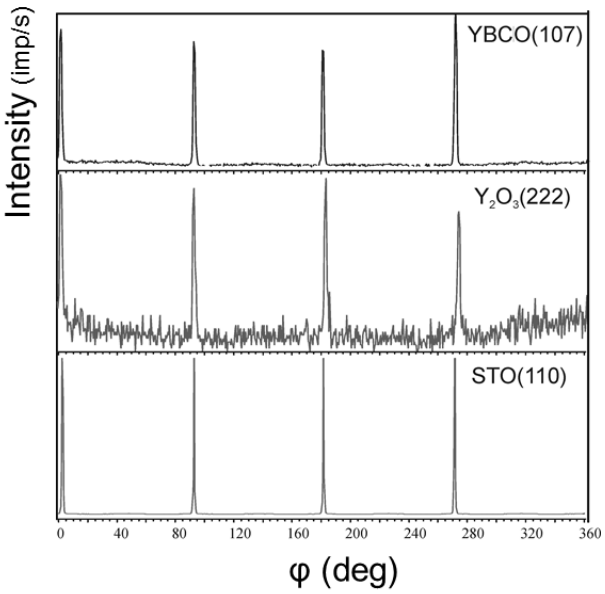

Fig. 4. XRD φ-scan of a YBCO film with Y_2O_3 inclusions

XRD θ-2θ-scans contained only (*h00*) reflections of yttrium oxide indicating that the phase grew oriented, with *a*-axis of the Y_2O_3 crystal lattice perpendicular to the substrate surface:

$$(001)\ Y_2O_3 \parallel (00l)\ \text{YBCO} \parallel (100)\text{STO}$$

XRD φ-scans clarified the in-plane orientation of Y_2O_3 (Fig. 4): (222) Y_2O_3 reflections were observed at

the same angles as (107) YBCO reflections, confirming the following epitaxial in-plane relation:

[110] Y_2O_3 || [100] YBCO

Figure 1 depicts the orientation of yttrium oxide in the YBCO matrix corresponding to the epitaxial relations we determined.

Using high-resolution electron microscopy (HREM), we found that Y_2O_3 grows in the YBCO matrix as nanosized (20x10 nm), densely distributed particles (Fig. 5). Co-orientation of the Y_2O_3 particles and YBCO matrix determined with HREM coincides with the XRD results.

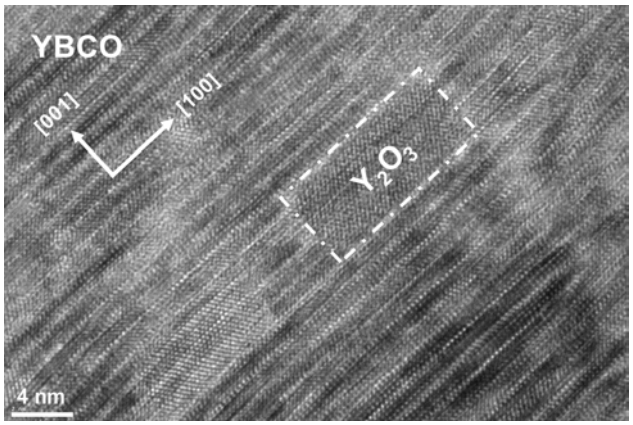

Fig. 5. HREM microphotograph of a YBCO film cross-section [8] showing a nanosized yttrium oxide inclusion in the YBCO matrix

XRD θ-2θ-scans of Y-poor films showed a peak of an impurity phase at $2\theta = 41.89°$ and grazing incidence XRD scans (2θ-χ-φ) of the same films showed 2 peaks at $2\theta = 41.89°$ and 44.53° (Fig. 6). We attributed these

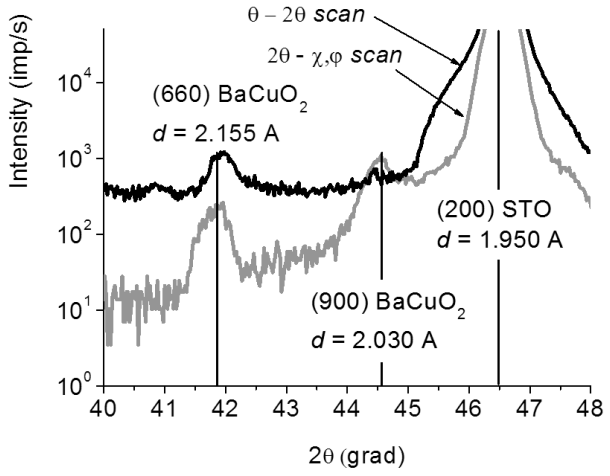

Fig. 6. XRD θ-2θ- and 2θ-χ, φ- (grazing incidence beam) scans of an Y-poor YBCO film containing the $BaCuO_2$ impurity phase

reflections to the $BaCuO_2$ phase (cubic lattice, Im3m, d = 18.27 Å), the peak at $2\theta = 41.89°$ corresponding to the (660) plane, and at $2\theta = 44.53°$ to the (009) plane. Since only the (660) reflection appeared in XRD θ-2θ-scans, we concluded that the $BaCuO_2$ phase grew oriented, with the [110] direction of the $BaCuO_2$ lattice parallel to the c-axis of YBCO:

[110] $BaCuO_2$ || [001] YBCO

It is noteworthy that the $BaCuO_2$ reflections were clearly seen in the grazing incidence (2θ-φ, χ) XRD scan, meaning that the $BaCuO_2$ crystals were located at the YBCO surface, similar to other low-melting barium cupric impurity phases, which are pushed to the top of the film during the step-flow growth of YBCO [9].

Y-rich films contained YBCO, Y_2O_3 and CuO_x phases. According to the bulk YBCO phase diagram, an equilibrium phase assembly cannot contain these three phases at the same time. However, in the thin film state these three phases can coexist due to epitaxial stabilization of Y_2O_3 in the YBCO matrix [10]. There have been numerous reports in the literature of coexistence of YBCO, Y_2O_3 and CuO_x in epitaxial YBCO films. Thin-film phase diagram in Fig. 7 summarizes our observations of phase assemblies in epitaxial YBCO films.

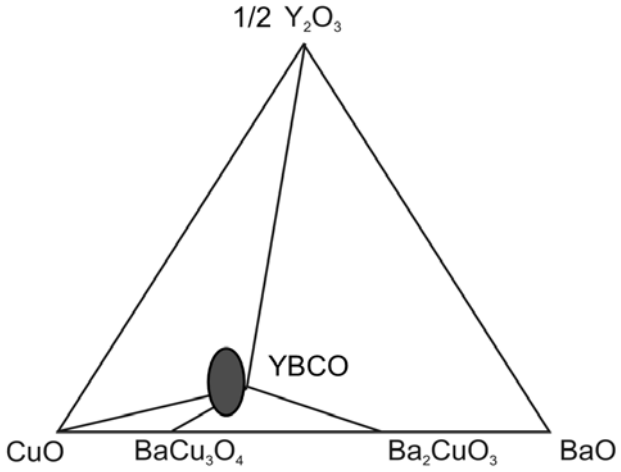

Fig. 7. Phase diagram of the Y_2O_3-BaO-CuO system for YBCO epitaxial films (T = 820 °C, $p(O_2)$ = 2 mbar) showing phase assemblies in the vicinity of the $YBa_2Cu_3O_{7-\delta}$ composition. Triangulation in the Ba-rich field is not available yet. The oval shows the range of compositions for the films discussed in this paper

STRAINED STATE OF Y_2O_3 PARTICLES IN THE YBCO MATRIX

Using XRD θ-2θ-scans we calculated the Y_2O_3 out-of-plane lattice parameter. It appeared that Y_2O_3

inclusions were compressed in the [001] direction, perpendicular to the substrate surface. The Y_2O_3 lattice parameter along this direction (parameter *c*) is 0.32—0.66% smaller than the bulk value (10.604 Å, cubic lattice). Since Y_2O_3 is a stoichiometric oxide and, therefore, the variation of its lattice parameter cannot be accounted for by a change in its oxygen content, its axial compression must be driven externally by the YBCO matrix.

Fig. 8 shows the observed linear dependence of the Y_2O_3 *c*-parameter on the YBCO *c*-parameter in the oxygenated films (the YBCO *c*-parameter varied in different oxygenated films due to slight deviation of oxygen content): larger YBCO *c*-parameter resulted in larger Y_2O_3 *c*-parameter.

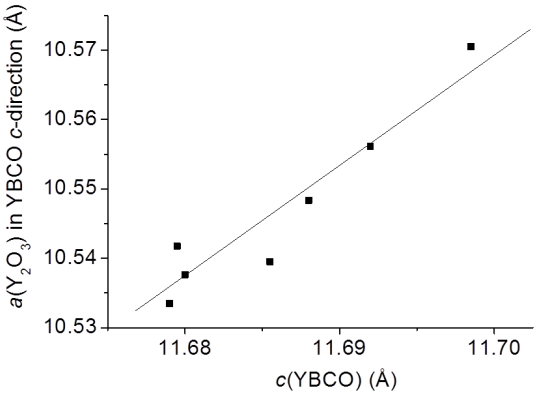

Fig. 8. Correlation between the YBCO *c*-parameter and the Y_2O_3 *c*-parameter, illustrating the elastic compression of the Y_2O_3 inclusions along *c*-axis in the YBCO matrix

We suggested that Y_2O_3 inclusions undergo compression by the YBCO matrix during YBCO oxygenation. To verify this suggestion, we ran a series of experiments with repeated reduction and oxygenation of the films.

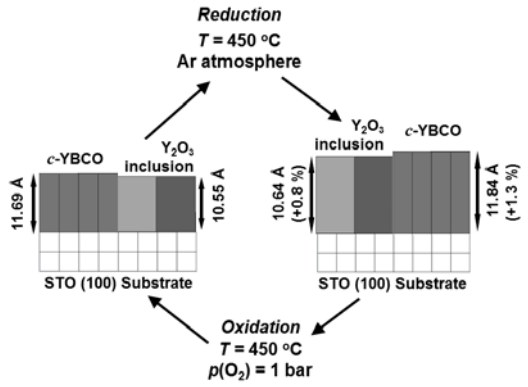

Fig. 9. Reversible compression and stretching of the Y_2O_3 inclusions during repeated oxygenation and reduction of the YBCO films

In oxygenated films, the YBCO *c*-parameter was 11.69 Å, and that of Y_2O_3 was 10.55 Å. After annealing of the films in 1 bar Ar YBCO was reduced and its lattice stretched along the *c*-axis by 1.3% to *c* = 11.84 Å. The structure of the Y_2O_3 particles stretched with the YBCO matrix (Fig. 9), so the Y_2O_3 out-of-plane *c*-parameter increased by 0.8% to 10.64 Å.

Such a behavior is possible because the Y_2O_3-YBCO interface along the *c*-direction is semi-coherent, and the Y_2O_3 epitaxial inclusions follow the change in the YBCO cell parameter caused by oxygenation and reduction of the YBCO structure.

INFLUENCE OF YTTRIUM OXIDE INCLUSIONS ON YBCO ORIENTATION

Authors in ref. [11] reported that in NdBCO films on STO (100) substrates *a*-oriented growth appeared when the films were deposited at relatively low temperatures, and the films were fully *c*-oriented at deposition temperatures above 730 ºC

We found, however, that in nearly stoichiometric MOCVD-derived YBCO films a mixture of *a*- and *c*-oriented YBCO grains grew even at 860 ºC, so there must be another driver for the formation of *a*-oriented YBCO besides temperature.

We analyzed the intensities of the YBCO and Y_2O_3 XRD peaks in the films. As shown in Fig. 10, the Y-rich films demonstrated much less tendency to *a*-oriented growth comparing to the Y-poor films, and even minor amount of Y_2O_3 in the film strongly suppressed *a*-oriented YBCO growth. This indicates that the ratio between the amount of *a*- and *c*-oriented YBCO grains depends on the cation stoichiometry of a film being deposited, namely on the phase field into which the film composition falls: Y-rich YBCO-Y_2O_3-CuO_x or Y-poor YBCO-$BaCuO_2$-CuO_x.

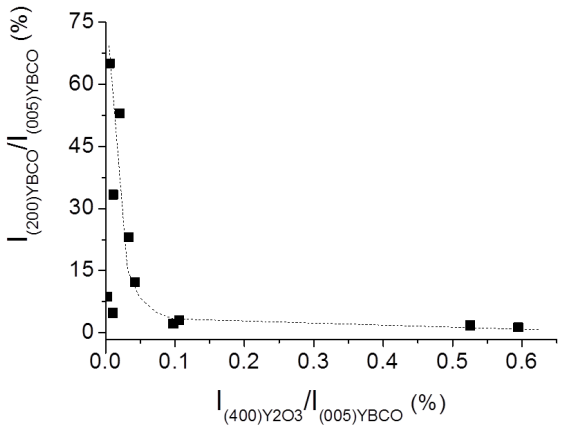

Fig. 10. Dependence between the relative XRD peak intensities of *a*-oriented YBCO and Y_2O_3. Even minor amount of Y_2O_3 in the film strongly suppresses *a*-oriented YBCO growth

Trying to understand the orientation behavior of YBCO films of different composition, we should consider the following two correlations generalized in ref. [12]: (1) growth of *c*-oriented YBCO is thermodynamically preferred because the (001) YBCO plane has the lowest surface energy, and (2) *a*-oriented YBCO growth occurs preferentially on very closely crystallographically matched substrates, such as STO (in-plane mismatch with *a*-oriented YBCO below 0.5%). Thus, a strong tendency to *a*-oriented YBCO growth is an intrinsic feature of YBCO films on the well-matched STO substrates.

Fundamentally, in both phase fields, YBCO-Y_2O_3-CuO_x and YBCO-$BaCuO_2$-CuO_x, the liquidus temperature is lower than that for stoichiometric YBCO, which results in higher diffusion mobility in the growing media of off-stoichiometric composition than in the stoichiometric media. This should make more favorable the growth of the thermodynamically preferred *c*-oriented YBCO grains in off-stoichiometric films.

On the other hand, in off-stoichiometric films the nature of secondary phases and localization of their crystallites with respect to the film surface and film-substrate interface play a very important role in the nucleation and growth of YBCO grains with certain orientation. As we discussed above, the $BaCuO_2$ crystallites localized mostly on the surface of the YBCO films, whereas the Y_2O_3 inclusions were uniformly distributed throughout the film. This difference in secondary phase localization could contribute to the difference in the ratio in *a*- and *c*-oriented YBCO grains in the Y-rich and Y-poor films.

In this paper, we limit ourselves to reporting the practically important result of intentional deposition of Y-rich films, in order to suppress *a*-oriented YBCO growth. Further extensive experiments are required to provide conclusive evidence of the nature and the mechanism of this phenomenon. That should become the subject of a future publication.

SUPERCONDUCTING PROPERTIES OF YBCO FILMS

A typical temperature dependence of magnetic susceptibility (real χ' and imaginary χ'' values) graph is shown in Fig. 11; we used these data to calculate the critical current density, J_c, of the films using the Bean model. Although oxygen content of YBCO is crucial for superconducting properties, J_c of the oxygenated films showed no dependence on the minor variations of the YBCO *c*-parameter, which reflected minor variations in the oxygen content. This means that the δ index variation in the $YBa_2Cu_3O_{7-\delta}$ formula in the

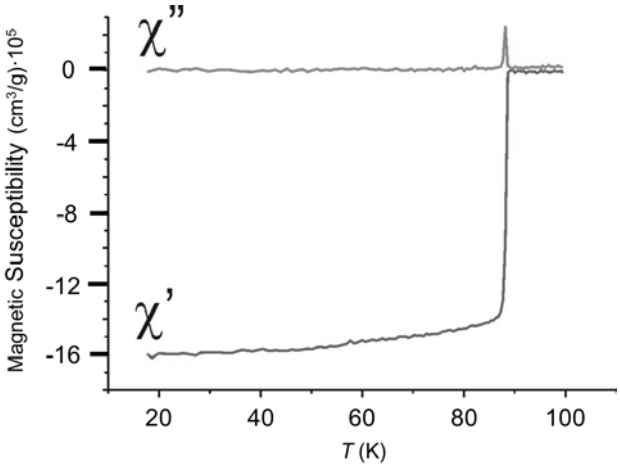

Fig. 11. Typical temperature dependence of magnetic susceptibility for a YBCO film

films was too small to affect superconductivity, but at the same time it was high enough to influence the Y_2O_3 *c*-parameter. The critical temperature of superconducting transition was 88 K for the majority of films with low or moderate Y_2O_3 content ($I_n(Y_2O_3) < 0.75\%$) (Fig. 12). The Y_2O_3-rich samples ($I_n(Y_2O_3) > 1.0\%$)

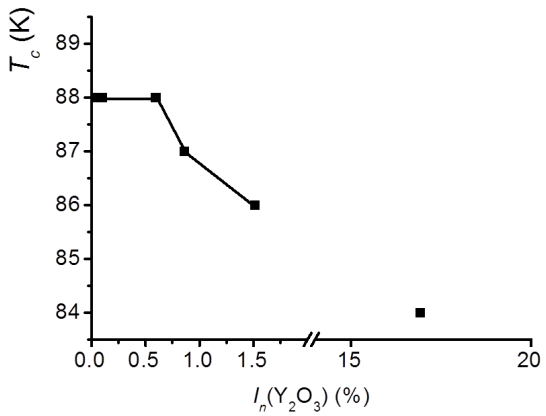

Fig. 12. Dependence of critical superconducting temperature on the Y_2O_3 content

had reduced T_c due to the appearance of weak links in the YBCO matrix caused by too many Y_2O_3 inclusions.

The dependence of J_c (measured at 77K and H=100 Oe) on the Y_2O_3 content is shown in Fig. 13: with increasing Y_2O_3 content, J_c increased from 0.5 to 0.9 MA/cm^2. Further increase of J_c was limited by the distortion of the YBCO matrix discussed above.

The dependence of J_c on the amount of *a*-oriented YBCO grains, I_n(*a*-YBCO), is shown in Fig. 14: with increasing I_n(*a*-YBCO), J_c dropped from 0.9 MA/cm^2 to very low values. As we show in this paper, Y_2O_3 inclusions suppress the formation of *a*-oriented YBCO,

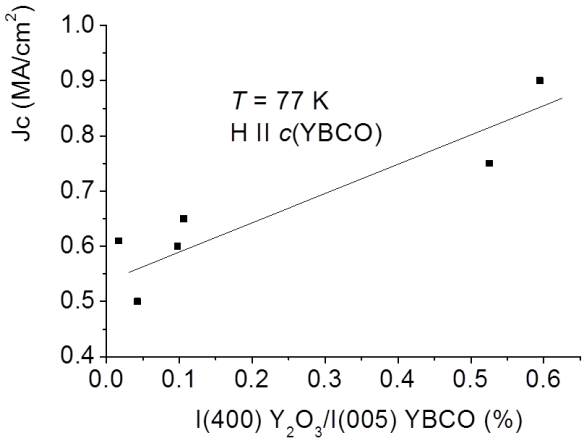

Fig. 13. Dependence of critical current at 77K (H=100 Oe) on the Y_2O_3 content

so the reason of the observed higher J_c in the Y-rich YBCO films is not solely the enhanced magnetic flux pinning on the Y_2O_3 particles, but also the higher degree of *c*-orientation in YBCO.

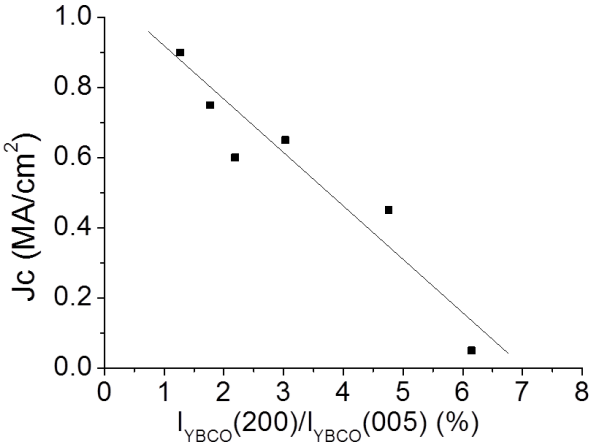

Fig. 14. Dependence of critical current 77K (H=100 Oe) on the amount of *a*-oriented YBCO grains

CONCLUSIONS

Studying the orientation and phase relations in the Y-Ba-Cu-O films prepared by MOCVD we observed a correlation between the presence of Y_2O_3 inclusions and the amount of *a*-oriented YBCO grains. The presence of yttrium oxide inclusions strongly influences the YBCO orientation, possibly due to different film growth mechanisms determined by the phase assembly in the crystalline film. As a result, Y-rich YBCO films grow highly textured, with complete domination of *c*-oriented YBCO. Y-poor films grow with a mixture of *a*- and *c*-oriented YBCO. Y-rich films demonstrate higher J_c values due to the better YBCO texture and enhanced magnetic flux pinning on the Y_2O_3 inclusions.

Y_2O_3 particles in YBCO films are strained due to their small size and strong bonding with the YBCO matrix provided by the semi-coherent epitaxial interface. In oxygenated YBCO films, Y_2O_3 particles are compressed in the *c* direction (normal to the substrate surface) in comparison to bulk Y_2O_3, and in reduced YBCO films Y_2O_3 particles are under tensile strain along the *c* direction. The stress state of the Y_2O_3 inclusions can be reversibly switched by performing oxygenating or reducing anneals.

Acknowledgements

The financial support from the Ministry of Education and Science of the Russian Federation under contract No. 16.523.11.3008 is acknowledged.

REFERENCES

1. *Iwasaki H., Inaba S., Sugioka K.,. et al.* // Physica C. 1997. V. 290. P. 113.

2. *Freyhardt H. C., Hellstrom E. E.* High-Temperature Superconductors: A Review of $YBa_2Cu_3O_{6+x}$ and (Bi, Pb) $_2Sr_2Ca_2Cu_3O_{10}$. Springer Verlag. 2007. 309 p.

3. *Dimos D., Chaudhari P., Mannhart J.* // Phys. Rev. B. 1990. V. 41. P. 4038.

4. *Murakami M., Gotoh S., Fujimoto H., et al.* // Supercond. Sci. Technol. 1991. V. 4. P. 843.

5. *Ni B., Kiuchi M., Otabe E. S.* // IEEE Trans. Appl. Supercond. 2003. V. 13. P. 3695.

6. *Broussard P. R., Cestone V. C., Allen L. H.* // IEEE Trans. Appl. Supercond. 1995. V. 5. P. 1222.

7. *Campbell T. A., Haugan T. J., Maartense I., et al.* // Physica C. 2005. V. 423. P. 1.

8. *Boytsova O. V., Samoilenkov S. V., Voloshin I. F., et al.* // Proceedings of EUCAS-2009.

9. *Samoylenkov S. V., Gorbenko O. Yu., Graboy I. E., et al.* // Chem. Mater. 1999. V. 11. P. 2417.

10. *Kaul A. R., Gorbenko O. Yu., Graboy I. E., et al.* // Chem. Mater. 2002. V. 14. P. 4026.

11. *Granozio F. M., Salluzzo M., Scotti di Uccio U., et al.* // Phys. Rev. B. 2000. V. 61. P. 1.

12. *Kaul A. R., Molodyk A. A., Samoilenkov S. V., et al.* // Proceedings of the MSU-HTSC. 1998.

Moyzykh Mikhail E. — postgraduate student, Department of Chemistry, Moscow State University; tel.: (495) 9390029, e-mail: moyzykh@gmail.com

Boytsova Olga V. — Doctoral Candidate, Department of Materials Science, Moscow State University; tel.: (495) 9390029, e-mail: boytsova@gmail.com

AmelichevVadim A. — Engineer, SuperOx-Innovations Company; tel.: (495) 6697995, e-mail: vadim.amelichev@gmail.com

Samoilenkov Sergey V. — Senior Staff Scientist, Institute of High Temperatures RAS, Director, SuperOx-Innovations Company; tel.: (495) 4858244, e-mail: ssv@superox.ru

Voloshin Igor F. — Leading Scientist, All-Russian Electrical Engineering Institute; tel.: (495) 3625617, e-mail: voloshin@vei.ru

Kaul Andrey R. — Professor, Department of Chemistry, Moscow State University, Research Supervisor, SuperOx-InnovationsCompany; e-mail: kaul@inorg.chem.msu.ru

Bertrand Lacroix — Maître de conferences, PôlePoitevin de Recherche pour l'Ingénieur en Mécanique, MatériauxetÉnergétique (PPRIMME), Departement de Physique et Mécanique des matériaux; tel.: (+33) 231452654, e-mail: bertrand.lacroix@ensicaen.fr

Fabien Paumier — Maître de conferences, PôlePoitevin de Recherche pour l'Ingénieur en Mécanique, MatériauxetÉnergétique (PPRIMME), Departement de Physique et Mécanique des matériaux; tel.: (+33) 549496747, e-mail: fabien.paumier@univ-poitiers.fr

Rolly J. Gaboriaud — Professor, PôlePoitevin de Recherche pourl'Ingénieur en Mécanique, Matériaux et Énergétique (PPRIMME), Departement de Physique et Mécanique des matériaux; tel.: (+33) 549496743, e-mail: rolly.gaboriaud@univ-poitiers.fr